

Response to Referee #2

The original comments are in regular text and our responses are in bold.

The authors have made good efforts to address the points raised in the review. The authors now present a quantitative conclusion and provide more justification for various decisions that have been made in setting up their simulations. The additional sensitivity tests that are now provided help to address my earlier concerns. As a result, the manuscript has been improved although it could further benefit from addressing the following minor points:

We thank the referee for the thoughtful review and respond to specific comments below.

Specific Comments:

P. 5 L.175-176 “These changes are small compared to the uncertainty in global OH.” I think a reference is needed here, perhaps Rigby et al. (2017) or Turner et al. (2017).

We add a reference to Rigby et al. (2017).

P.7 L228-229 – Thank you for providing this new Fig 6. which is certainly useful, but could you please provide a brief explanation for why the isotope ratio is overestimated at BRW in contrast to other sites. Is it likely to be due to an incorrect latitudinal distribution of sinks, sources or even transport errors?

Most of our simulations underestimate the latitudinal gradient of $\delta^{13}\text{CH}_4$, leading to the overestimate at BRW compared to the other sites, even though they reproduce well the interhemispheric gradient of total CH_4 . While multiple factors may contribute, the SimWet simulation, which uses spatially varying isotopic ratios for wetland emissions, gives a reasonable reproduction of the $\delta^{13}\text{CH}_4$ observations at both BRW and the southernmost site, SPO. This suggests that latitudinal variability in the isotopic source ratios, which is absent in the other simulations, contributes to the bias at BRW compared to the other stations. We add the following text to Section 3.4:

“SimWet is better able to simultaneously match the $\delta^{13}\text{C}$ - CH_4 observations at both the northernmost (BRW) and southernmost (SPO) sites shown in Fig. 6 than the other simulations, even though all simulations reproduce the latitudinal distribution of CH_4 well (Fig. 4). This highlights the importance of spatially varying isotopic ratios for the $\delta^{13}\text{C}$ - CH_4 distribution.”

Technical Corrections:

P. 3 L 100 – Missing ‘of’ in “understanding the impacts [of] inter-model differences”

Fixed

P. 5 L180 – “which uses the same Cl field as Cl but retains”. Is this meant to say “SimTOM” in place of the second “Cl” perhaps?

Yes, we changed it to “SimTom”.

P. 8 L286 – “for each [1]% increase in CH₄ loss by Cl.” Missing 1.

We added the “one”.

Strong Sensitivity of the Isotopic Composition of Methane to the Plausible Range of Tropospheric Chlorine

Sarah A. Strode^{1,2,*}, James S. Wang^{1,2,**}, Michael Manyin^{2,3}, Bryan Duncan², Ryan Hossaini⁴, Christoph A. Keller^{1,2}, Sylvia E. Michel⁵, James W. C. White⁵

¹Universities Space Research Association, Columbia, MD, USA

²NASA Goddard Space Flight Center, Greenbelt, MD, USA

³SSAI, Lanham, MD, USA

⁴Lancaster Environment Centre, Lancaster University, Lancaster, UK

⁵Institute of Arctic and Alpine Research, University of Colorado, Boulder, CO, USA

*correspondence to: sarah.a.strode@nasa.gov

**Now at the Institute for Advanced Sustainability Studies, Potsdam, Germany

Abstract. The ^{13}C isotopic ratio of methane, $\delta^{13}\text{C}$ of CH_4 , provides additional constraints on the CH_4 budget to complement the constraints from CH_4 observations. The interpretation of $\delta^{13}\text{C}$ observations is complicated, however, by uncertainties in the methane sink. The reaction of CH_4 with Cl is highly fractionating, increasing the relative abundance of $^{13}\text{CH}_4$, but there is currently no consensus on the strength of the tropospheric Cl sink. Global model simulations of halogen chemistry differ strongly from one another in terms of both the magnitude of tropospheric Cl and its geographic distribution. This study explores the impact of the inter-model diversity in Cl fields on the simulated $\delta^{13}\text{C}$ of CH_4 . We use a set of GEOS global model simulations with different predicted Cl fields to test the sensitivity of the $\delta^{13}\text{C}$ of CH_4 to the diversity of Cl output from chemical transport models. We find that $\delta^{13}\text{C}$ is highly sensitive to both the amount and geographic distribution of Cl . Simulations with Cl providing 0.28% or 0.66% of the total CH_4 loss bracket the $\delta^{13}\text{C}$ observations for a fixed set of emissions. Thus, even when Cl provides only a small fraction of the total CH_4 loss and has a small impact on total CH_4 , it provides a strong lever on $\delta^{13}\text{C}$. Consequently, it is possible to achieve a good representation of total CH_4 using widely different Cl concentrations, but the partitioning of CH_4 loss between the OH and Cl reactions leads to strong differences in isotopic composition depending on which model's Cl field is used. Comparing multiple simulations, we find that altering the tropospheric Cl field leads to approximately a 0.5‰ increase in $\delta^{13}\text{C}$ for each percent increase in how much CH_4 is oxidized by Cl . The geographic distribution and seasonal cycle of Cl also impacts the hemispheric gradient and seasonal cycle of $\delta^{13}\text{C}$. The large effect of Cl on $\delta^{13}\text{C}$ compared to total CH_4 broadens the range of CH_4 source mixtures that can be reconciled with $\delta^{13}\text{C}$ observations. Stronger constraints on tropospheric Cl are necessary to improve estimates of CH_4 sources from $\delta^{13}\text{C}$ observations.

1. Introduction

The global budget of methane is of great interest due to methane's role as a greenhouse gas, ozone precursor, and sink of the hydroxyl radical. Despite extensive study, major uncertainties in the methane budget remain, with top-down and bottom-up estimates often yielding different results (Kirschke et al., 2013; Saunio et al., 2016; Saunio et al., 2017, and refs therein) for the strength of specific source types. Furthermore, the resumed increase of methane concentrations beginning in 2007 (Dlugokencky et al., 2009; Rigby et al., 2008) can be explained by multiple hypotheses including an increase in fossil fuel emissions (Turner et al., 2016; Thompson et al., 2015; Hausmann et al., 2016), an increase in fossil fuel emissions combined with a decrease in biomass burning (Worden et al., 2017), an increase in biogenic sources (Schaefer et al., 2016; Nisbet et al., 2016), or a decrease in hydroxyl concentrations (Turner et al., 2017; Rigby et al., 2017). Variations in hydroxyl concentrations may also be important for the decrease in methane growth from 1999-2006 (McNorton et al., 2016).

Observations and modeling of methane's carbon isotopes provides additional information on methane sources since individual sources differ in their ^{13}C to ^{12}C ratio ($\delta^{13}\text{C}$). Isotopic information can be used to better constrain methane sources (e.g. Thompson et al., 2015; Mikaloff Fletcher et al., 2004b, a) and infer how the source mixture changed over glacial (e.g. Hopcroft et al., 2018; Fischer et al., 2008; Bock et al., 2017), millennial (e.g. Ferretti et al., 2005; Houweling et al., 2008), and decadal timescales (e.g. Nisbet et al., 2016; Schaefer et al., 2016; Kai et al., 2011; Schwietzke et al., 2016; Thompson et al., 2018). However, there are considerable uncertainties in the processes that control methane's isotopic composition that may confound source apportionment studies. Many modeling studies use a single value for the isotopic ratio of each source, while in reality sources such as wetlands, biomass burning, and natural gas show large regional or environment-dependent variations in their isotopic signature (Ganesan et al., 2018; Brownlow et al., 2017; Dlugokencky et al., 2011; Schwietzke et al., 2016; Sherwood et al., 2017).

The isotopic composition of atmospheric methane is also sensitive to methane's sinks. Reaction with OH, the principal loss for atmospheric methane, has a kinetic isotope effect (KIE) of -5.4‰ ($\alpha=k_{13}/k_{12}=0.9946$) to -3.9‰ ($\alpha=0.9961$) (Saueressig et al., 2001; Cantrell et al., 1990) and contributes to the interhemispheric gradient of $\delta^{13}\text{C}$ (Quay et al., 1991). Mass balance (Lassey et al., 2007) and observations of the seasonal cycle of $\delta^{13}\text{C}$ versus methane concentration, however, suggest larger apparent KIE values, which may indicate a role for methane oxidation by chlorine (Cl) in the marine boundary layer (MBL) (Allan et al., 2001; Allan et al., 2007) since Cl has a KIE of -61.9‰ ($\alpha=0.938$) at 297K (Saueressig et al., 1995). Inclusion of the MBL Cl sink alters the source mixture inferred from inverse modeling of $\delta^{13}\text{CH}_4$ (Rice et al., 2016). Nisbet et al. (2019) point out that interannual variability in the CH_4 Cl sink could explain some of the variability of $\delta^{13}\text{C}$. Cl is also an important methane sink in the stratosphere, and the impact of this sink on surface $\delta^{13}\text{C}$ is a source of uncertainty in modeling $\delta^{13}\text{C}$ (Ghosh et al., 2015). Reaction with stratospheric Cl contributes approximately 0.23‰ to the $\delta^{13}\text{C}$ of surface methane and makes a small contribution to the observed trend in surface $\delta^{13}\text{C}$ over the last century (Wang et al., 2002).

The global concentration of Cl in the MBL and its role in the methane budget is still uncertain. Cl concentrations are highly variable and not well constrained by direct observations. Modeling work by Hossaini et al. (2016) and Sherwen et al. (2016) suggests that chlorine provides 2-2.5% of tropospheric methane oxidation. This

agrees well with estimates based on the isotopic fractionation, which also suggest Cl provides several percent of the total sink (Allan et al., 2007; Platt et al., 2004). However, Gromov et al. (2018) suggest that these are overestimates as values over 1% are inconsistent with the $\delta^{13}\text{C}$ of CO, which is a product of CH₄ oxidation. The recent modeling study of Wang et al. (2019) also suggests a value of 1%. There is thus considerable uncertainty in the role of chlorine in the budget and isotopic composition of methane.

Here, we investigate the sensitivity of $\delta^{13}\text{C}$ of CH₄ to inter-model diversity in tropospheric chlorine concentrations to better quantify how much uncertainty in the interpretation of $\delta^{13}\text{C}$ is imposed by the uncertainty in Cl. Section 2 describes the modeling framework. We present results for total CH₄ and its isotopic composition compared to surface observations in Section 3, and discuss the implications for the global CH₄ budget in Section 4.

2. Methods

2.1 Model Description

We simulate atmospheric methane with the Goddard Earth Observing System (GEOS) global earth system model (Molod et al., 2015; Nielsen et al., 2017). The model has 72 vertical levels extending from the surface to 1 Pa. We conduct simulations at C90 resolution on the cubed sphere, which corresponds to approximately 100 km horizontal resolution. The simulations' meteorology is constrained to the MERRA-2 reanalysis (Gelaro et al., 2017) using a "replay" method (Orbe et al., 2017). The GEOS replay agrees well with the tropospheric mean age of the Global Modeling Initiative (GMI) chemistry and transport model (CTM) (Orbe et al., 2017), which shows reasonable agreement with the age derived from SF₆ observations, albeit with an old bias in the southern hemisphere (Vaugh et al., 2013). We thus expect the simulated interhemispheric transport time to be reasonable.

The GEOS CH₄ simulation can be interactively coupled to CO and OH (Elshorbany et al., 2016), or run independently with prescribed OH fields. We take the latter approach in this study, since this approach is able to capture many of the observed variations in atmospheric methane (Elshorbany et al., 2016). We prescribe the OH field following (Spivakovsky et al., 2000), but modify the OH to be approximately 20% higher in the Northern Hemisphere than the Southern Hemisphere, consistent with the OH field produced by many global atmospheric chemistry models (Naik et al., 2013; Strode et al., 2015). This modification is designed to make our results more applicable to understanding the impacts of inter-model differences in Cl, since it makes our OH distribution more consistent with that produced by many CCMs. The OH field varies monthly but repeats every year. We also include stratospheric losses for CH₄ from reaction with OH, Cl, and O¹D. These fields are prescribed from output of the GMI CTM (<https://gmi.gsfc.nasa.gov>) (Strahan et al., 2007; Duncan et al., 2007).

We implement the CH₄ isotopes in GEOS by separately simulating ¹³CH₄ and ¹²CH₄ tracers. We then calculate total CH₄ as the sum of the two carbon isotopologues and calculate $\delta^{13}\text{C}$ of CH₄ in per mil using the standard definition:

$$\delta^{13}\text{C-CH}_4 (\text{‰}) = ([^{13}\text{CH}_4]/[^{12}\text{CH}_4]/R_{\text{std}} - 1) * 1000 \quad (1)$$

where $R_{\text{std}}=0.0112372$ is the peedee belemnite isotopic standard (Craig, 1957). We partition each emission source into ¹²CH₄ and ¹³CH₄ emissions according to a source-specific $\delta^{13}\text{C}$ value from the literature, provided in Table 1. We use the Craig (1957) R_{std} value to partition the sources since it is cited in the literature used in Table 1 (Houweling et

Deleted: by

al, 2000; Lassey, 2007), and so for consistency we use the same value in equation 1 to calculate the simulated $\delta^{13}\text{C}$ of the CH_4 concentrations. We note, however, that the GMD observations now use a slightly different standard, the VPDB value of 0.011183 (Zhang and Li, 1990). A sensitivity study (not shown) confirms that the choice Rstd has little effect on our results as long as the same value is used for the source partitioning as for the calculation of $\delta^{13}\text{C}$ - CH_4 from simulated $^{13}\text{CH}_4$ and $^{12}\text{CH}_4$.

The reaction rates for CH_4+OH , CH_4+Cl , and $\text{CH}_4+\text{O}^1\text{D}$ differ between the $^{12}\text{CH}_4$ and $^{13}\text{CH}_4$ simulations to account for the kinetic isotope effect (KIE). In particular, we assume α values of 0.987 and 0.938 for $\text{CH}_4+\text{O}^1\text{D}$ and CH_4+Cl , respectively (Saueressig et al., 1995; Saueressig et al., 2001). Our standard simulation uses $\alpha_{\text{OH}} = 0.9946$ (Cantrell et al., 1990).

Methane from different sources is tracked individually using a “tagged tracer” approach, which allows us to simulate the spatial footprint of CH_4 and $\delta^{13}\text{C}$ - CH_4 from individual sources. The soil sink is applied to each tracer as a fraction of its source, modified to account for faster loss of $^{12}\text{CH}_4$ to soil compared to $^{13}\text{CH}_4$ ($\alpha_{\text{soil}} = 0.978$) (Tyler et al., 1994). Supplemental figure S1 shows the July 2004 CH_4 and $\delta^{13}\text{C}$ - CH_4 footprints of the biomass burning, wetland, and coal + other geologic CH_4 sources from the tagged tracers to illustrate the tagged tracer approach. We note that the $\delta^{13}\text{C}$ values of the surface methane from each source is heavier (less negative) than the emission value for that source (Table 1), especially in regions far from the source, because of the fractionating effects of the sinks. Supplemental Fig. S2 shows the corresponding footprints for January.

2.2 Description of Simulations

We simulate the period from 1990 through 2004, and focus our analysis on 2004. We choose 2004 as our endpoint because it lies within the period when methane concentrations remained relatively flat, simplifying our analysis. Ending the simulations in 2004 also avoids much of the uncertainty about the causes of the resumed growth rate in recent years. The isotopic ratios of methane take longer to adjust to a perturbation than total methane (Tans, 1997). Since we wish to begin our simulations with a state that is as close as possible to “spun up”, we choose the initial condition for each tagged tracer based on its present-day distribution and proportion of the total CH_4 and scale it back to 1990 levels such that the total CH_4 is consistent with the global mean CH_4 from surface observations for 1990. We then iteratively adjusted the ^{12}C - to ^{13}C - CH_4 tracer ratios at the beginning of 1990 to yield a good match to global mean $\delta^{13}\text{C}$ - CH_4 observations for 1998, when more $\delta^{13}\text{C}$ - CH_4 observations are available. The same initial condition is used for the standard and sensitivity simulations.

We use interannually-varying emissions of CH_4 from anthropogenic, biomass burning, and wetland sources. Emissions from anthropogenic sources such as oil and gas, energy production, industrial activities, and livestock come from the EDGAR version 4.2 inventory (European Commission, 2011). Biomass burning emissions come from the MACCity inventory (Granier et al., 2011). We treat forest fires as C3 burning and savannas as C4 burning for partitioning the biomass burning emissions between isotopologues. Wetland and rice emissions come from the Vegetation Integrative Simulator for Trace gases (VISIT) terrestrial ecosystem model (Ito and Inatomi, 2012), scaled by 0.69 and 0.895, respectively, for consistency with the Transcom- CH_4 study (Patra et al., 2011). Ocean (Houweling et al., 1999), termite (Fung et al., 1991), and mud volcano emissions (Etiope and Milkov, 2004) are also from the

Transcom study (Patra et al., 2011) and have a seasonal cycle but no interannual variability. Initial tests with these emissions showed a substantial underestimate of the CH₄ growth rate. Consequently, we scale up all the emissions by 10% for 1990-1998, and by 6.8% for 1998-2004. We find the resulting emissions lead to a good simulation of the timeseries of surface CH₄ observations from the National Oceanic and Atmospheric Administration (NOAA) Global Monitoring Division (GMD) (Dlugokencky et al., 2018), especially towards the end of the period (Fig. 1). The simulation has only a 0.1% mean bias compared to the observations for 2004.

Our standard simulation (SimStd) uses Cl from the GMI CTM for the tropospheric as well as stratospheric loss of CH₄ by reaction with Cl. Tropospheric Cl concentrations are small in GMI since it does not include very short-lived species, and reaction with Cl represents only 0.28% of the total tropospheric CH₄ loss. We also conduct several sensitivity simulations in which we alter the tropospheric and lower stratospheric Cl fields (Table 2). Cl is not altered above 56 hPa. Sensitivity simulation SimGC uses Cl from the GEOS-Chem chemistry module within GEOS (Long et al., 2015; Hu et al., 2018). GEOS-Chem v11-02f with fully coupled tropospheric and stratospheric chemistry was used for this simulation, with halogen chemistry as described in Sherwen et al. (2016). SimGC has higher values of tropospheric Cl than SimStd (Figs. 3,4) and leads to 0.66% of the total CH₄ loss occurring via Cl. Both SimStd and SimGC are thus below the 1% loss via Cl suggested by (Gromov et al., 2018). We conduct a third sensitivity simulation, SimTom, which uses Cl from the TOMCAT model simulations that include chlorine sources from chlorocarbons (including very short-lived substances), HCl from industry and biomass burning, and very short lived substances (Hossaini et al., 2016). This simulation leads to Cl accounting for 2.5% of tropospheric CH₄ loss in our simulation. Finally, we conduct a fourth sensitivity simulation, SimMBL, which modifies the Cl over the oceans at altitudes below 900 hPa (Fig. 2d) to reflect the marine boundary layer distribution suggested by (Allan et al., 2007). This Cl field is described by the following equation:

$$Cl_MBL = 18 \times 10^3 \text{ atoms/cm}^3 * (1 + \tanh(3\lambda) * \sin(2\pi * (t-90)/365)) \quad (2)$$

where λ is latitude in radians and t is the day of the year. Elsewhere SimMBL uses the Cl field from SimStd. This simulation has the highest percent of CH₄ loss occurring via Cl: 3.9%. If we consider the loss of methane throughout the atmosphere rather than just the troposphere, then the percent lost via Cl increases to 1.6%, 2.0%, 3.6% and 5.0% for SimStd, SimGC, SimTom, and SimMBL, respectively.

We designed the sensitivity experiments to alter the isotopic composition of CH₄ without greatly affecting the total CH₄. Consequently, we reduce the OH concentrations in the SimTom and SimMBL simulations by 2% and 4%, respectively, relative to the SimStd OH to offset the effect of increasing Cl. These changes are small compared to the uncertainty in global OH (Rigby et al., 2017). In addition, the SimTom and SimMBL simulations use $\alpha_{OH}=0.9961$ (Saueressig et al., 2001) rather than $\alpha_{OH}=0.9946$ (Cantrell et al., 1990) to avoid too much fractionation from the combined Cl and OH sinks. While these changes are necessary to maintain consistent total CH₄ and reasonable isotopic ratios, changing multiple factors in addition to Cl makes it difficult to quantify the impact of Cl alone. Consequently, we conduct an additional sensitivity study, called SimTomB, which uses the same Cl field as SimTom, but retains the OH and α_{OH} values of SimStd. SimTomB is used in Section 3.3. This simulation becomes too heavy compared to observations, justifying the need to change α_{OH} in the main SimTom simulation. We also

Formatted: Subscript

Deleted: Cl

conduct a sensitivity simulation, SimOHp, that uses the same CI field as SimStd but does not alter the hemispheric ratio of OH. Table 2 summarizes the standard and sensitivity simulations.

The four CI distributions differ in their vertical and horizontal spatial distributions as well as their tropospheric mean (Figs. 2 and 3). The SimStd CI is largest in the tropics, nearly symmetric between hemispheres, and increases with altitude. Both SimGC and SimTom have CI that is larger in the Northern Hemisphere than the Southern Hemisphere in the annual mean and reaches a minimum in the mid-troposphere. However, the maximum in lower tropospheric CI occurs in the tropics in SimGC but in the extratropics in SimTom. This mid-latitude CI maximum arises because SimTom has high CI values over east Asia, whereas SimGC CI is highest over ocean regions (Fig. 3). SimMBL has a strong maximum in the MBL compared to the free troposphere and land regions. Its annual mean CI concentrations are higher in the Southern Hemisphere (Fig. 2) due to the larger ocean area in the Southern Hemisphere. However, SimMBL includes a strong seasonal shift in peak CI between the hemispheres. SimStd and SimGC have more modest seasonal shifts, while CI in SimTom remains concentrated in the northern hemisphere throughout the year (Fig. S3). All simulations repeat the same CI field from year to year.

The sensitivity simulations listed above are designed to test the role of the CI sink. We conduct an additional sensitivity study, SimWet, to illustrate the role of spatial variation in the isotopic source signature. SimWet parallels SimStd, but the isotopic composition of the wetland source uses spatial variation from Ganesan et al (2018). The global mean source signature of the wetland emissions remains -60‰.

2.3 Observations

We use surface observations from the NOAA GMD Carbon Cycle Cooperative Global Air Sampling Network to evaluate our simulations. We use the monthly mean observations of total CH₄ (Dlugokencky et al, 2018) and $\delta^{13}\text{C}$ of CH₄ (White et al., 2018) to compare to the monthly mean simulation results. The isotopic measurements were made at the Institute of Arctic and Alpine Research at the University of Colorado and are referenced to the VPDB scale (Zhang and Li, 1990). The analytical uncertainty of the isotopic measurements is 0.06‰. The variability between measurements taken in a given month may, however, be larger, so we use the maximum of analytical uncertainty and the within-month standard deviation as the uncertainty in the monthly mean. When multiple years are observations are averaged together, we use the pooled variance to calculate the standard error, thus reducing the error based on the number of years. The GMD observations are located at remote sites, shown in Fig. 4 for CH₄ in 2004. Measurements of $\delta^{13}\text{C}$ of CH₄ are available at a subset of the sites, shown in Fig. 5.

3. Results and Discussion

3.1 Evaluation of Simulated CH₄

We find good agreement between the SimStd simulation and the GMD observations for CH₄ (Fig. 4) for 2004. We focus on these two months to represent the seasonal differences. The latitudinal distribution is well-reproduced, and the simulation captures the elevated concentrations of CH₄ observed over Europe in January as well as the January versus July differences in concentration. Overall, the spatial correlation between SimStd and the observations is 0.93

in January and 0.85 in July. The sensitivity simulations described in Table 2 have little effect on the CH_4 distribution, as shown by the overlapping symbols in Fig. 4c,d.

3.2 Impact of CI on the $\delta^{13}\text{C}$ Distribution

We next examine the distribution of $\delta^{13}\text{C}$ in SimStd compared to observations. Figure 6 shows the timeseries of observed and simulated $\delta^{13}\text{C}$ for 1998-2004 at the 6 GMD sites with $\delta^{13}\text{C}$ records covering this time period. We begin the figure at 1998 rather than 1990 due to the lack of data availability in the earlier years. The standard and sensitivity simulations overestimate $\delta^{13}\text{C}$ at the northernmost station, BRW. The observations at the other stations lie within the range of simulations, with most simulations underestimating the observations at the south pole. The differences between the different sensitivity simulations are large compared to the interannual variability in both observed and simulated $\delta^{13}\text{C}$. We focus our subsequent analysis on a single year, 2004.

Fig. 5a,b shows both meridional and zonal variability in $\delta^{13}\text{C}$. Background values are less negative (heavier) in the Southern versus Northern Hemisphere (NH) (Fig. 7), a feature seen more strongly in the observations, but there is also variability due to the different source signatures. Areas of biomass burning, such as Tropical Africa, show up as particularly heavy, while regions with large wetland and rice emissions, such as SE Asia, are particularly light. Another prominent feature is the isotopically heavy region in northern Eurasia (around 60°N) in January, which we attribute to the influence of the geologic (including oil, gas, and coal) source in this region (Supp. Fig. S2). This signal is less evident in July, when greater influence from boreal wetlands lightens the isotopic mix. The spatial correlation (r^2) between the SimStd and observed $\delta^{13}\text{C}$ is 0.61 in January and 0.75 in July.

The sensitivity simulations with altered oxidant concentrations alter the global values of $\delta^{13}\text{C}$, but the geographic patterns remain similar to that of SimStd. The larger CI sink in SimGC leads to an overall less negative $\delta^{13}\text{C}$, which agrees better than SimStd with observations at Southern Hemisphere (SH) sites but worse in the NH (Figs. 6c,d and 7). The isotopic effect of the larger CI sink in SimTom is compensated by the lower OH and α_{OH} values used in that simulation, flattening the interhemispheric gradient (Figs. 6e,f and 7). In contrast, the very large MBL CI concentrations in SimMBL lead to an overestimate (insufficiently negative) of the observed $\delta^{13}\text{C}$ (Fig. g,h), but strengthens the interhemispheric gradient. We note that since all simulations began with the same initial conditions but have different sinks, the isotopic composition is not in steady state in 2004 and the results of the sensitivity simulations diverge further with additional years of simulation, with SimMBL becoming clearly inconsistent with observations. We note that while these results highlight the differences in $\delta^{13}\text{C}$ imposed by changing CI, the absolute values of $\delta^{13}\text{C}$, and hence their agreement with observations, would be different for CH_4 source mixtures with a different average $\delta^{13}\text{C}$.

Figure 7 reveals an underestimate in the interhemispheric gradient of $\delta^{13}\text{C}$ in both SimStd and the sensitivity runs compared to the GMD observations. Table 3 presents the observed and simulated $\delta^{13}\text{C}$ interhemispheric gradients calculated as the difference between the $\delta^{13}\text{C}$ values averaged over all sites south of 30°S and the average over sites north of 30°N . SimStd and SimGC show similar underestimates of the observed gradient, and the underestimate is more severe in SimTom. The gradient is improved in SimMBL in January. The differences between simulations

reflect differences in the locations where CH₄ oxidation occurs and the amount and location of isotopic fractionation due to Cl versus OH. Fig. 8 shows that the higher Cl values over the NH, particularly China, in SimTom versus SimStd leads to more CH₄ loss occurring in the NH and higher (heavier) $\delta^{13}\text{C}$ in the NH. This effect is particularly pronounced over China and Europe. Less fractionation by the OH sink in SimTom leads to lighter values in the SH. Conversely, SimMBL has more loss occurring over the SH oceans in January, leading to heavier $\delta^{13}\text{C}$ in the SH (Fig. 9). This effect is not present in July, when the SimMBL Cl loss shifts to the NH (Fig. S4). The reduced hemispheric difference in OH in SimOHp leads to a small improvement in the hemispheric gradient in $\delta^{13}\text{C}$.

We further examine the seasonal cycle of $\delta^{13}\text{C}$ in Fig. 10. We focus on the seasonal cycle at the South Pole Observatory (SPO) site because it is far from large CH₄ sources and thus the seasonal cycle depends strongly on the seasonality of the CH₄ sinks. While all simulations lie mostly within the error bars of the observations, SimMBL has the largest seasonal cycle amplitude, overestimating the seasonal cycle at of the SPO observations with a $\delta^{13}\text{C}$ value that is both too heavy in Feb.-June and too light in Aug.-Nov. In contrast, SimStd and the other sensitivity simulations underestimate the magnitude of the observed seasonal cycle at SPO. Supplemental Fig. S5 shows a large enhancement in the seasonal cycle amplitude between SimMBL and the other simulations for the Cape Grim site in Tasmania (CGO), but only a small change at other sites. This suggests that while MBL Cl is attractive as an explanation for the SH seasonality of $\delta^{13}\text{C}$, this explanation may be inconsistent with the inclusion of non-marine Cl sources. However, since the seasonal cycle amplitude at SPO lies in between SimMBL and the other simulations, it is possible that an MBL Cl source similar to that of SimMBL but with a smaller average value could reproduce the amplitude well.

3.3 Quantifying the Sensitivity of $\delta^{13}\text{C}$ to CH₄ Loss by Cl

Given the substantial range in estimates for how much methane is lost by reaction with tropospheric Cl, it is important to quantify the sensitivity of global mean surface $\delta^{13}\text{C}$ to the CH₄ loss by Cl. This analysis summarizes the global impact of the isotopic effect of the Cl differences between simulation discussed above. Fig. 11 shows the global mean, area weighted surface $\delta^{13}\text{C}$ in 2004 as a function of the percent of CH₄ oxidized by Cl for SimStd, SimGC, and SimTomB the three simulations with the same OH and emissions but different Cl. A strong linear relationship is evident between the oxidation by Cl and the surface $\delta^{13}\text{C}$. The slope of the linear regression line indicates the expected increase in surface $\delta^{13}\text{C}$ for a change in the percent of CH₄ oxidized by Cl. Based on this analysis we expect that surface $\delta^{13}\text{C}$ will increase by approximately 0.5‰ for each one % increase in CH₄ loss by Cl.

3.4 Sensitivity of $\delta^{13}\text{C}$ to the Isotopic Distribution of Sources

Other factors in addition to the Cl distribution likely contribute to the mismatch between the observed and simulated interhemispheric gradients. Fig. 5 shows the impact of the geologic source on the $\delta^{13}\text{C}$ values over northern Asia. A bias in either the strength or the isotopic composition of this source will impact the interhemispheric gradient. Another likely contributing factor is our use of a globally uniform isotopic ratio for each source type. Ganesan et al.

(2018) developed a global map of the isotopic signatures of wetland emissions. We use this map to impose spatially varying isotopic ratios on our SimWet simulation. SimWet increases the amplitude of the seasonal cycle in $\delta^{13}\text{C}$ -CH₄ particularly for northern latitudes sites such as ALT, BRW, and MHD (Supplemental Fig. S5). It has little effect on the seasonal cycle at the SH CGO and SPO sites, where SimMBL shows a large effect on the cycle. SimWet results in improved agreement with the observed interhemispheric gradient (Figs. 5,7; Table 3). SimWet is better able to simultaneously match the $\delta^{13}\text{C}$ -CH₄ observations at both the northernmost (BRW) and southernmost (SPO) sites shown in Fig. 6 than the other simulations, even though all simulations reproduce the latitudinal distribution of CH₄ well (Fig. 4). This highlights the importance of spatially varying isotopic ratios for the $\delta^{13}\text{C}$ -CH₄ distribution. The size of the effect of including spatially varying ratios in wetland emissions depends on the strength of the wetland emissions as well as the other sources. Including spatially-varying isotopic signature for other sources as well could further modify the simulated interhemispheric gradient, potentially correcting some of the flat gradient of e.g. the SimTom simulation.

Formatted: Subscript

4. Conclusions

The role of Cl as a methane sink is a significant uncertainty in the global CH₄ budget, particularly with respect to isotopes. The global distribution of Cl is not well known from observations, and the Cl distributions simulated by global models varies widely from model to model. We investigated the sensitivity of the surface $\delta^{13}\text{C}$ distribution of CH₄ to the inter-model diversity in tropospheric Cl using a series of sensitivity studies with a global 3D model. Given the uncertainties in CH₄ sources and their isotopic ratios, it is not possible to conclude from this study which Cl field is best. However, the differences between the simulations provides insight on the strong lever that tropospheric Cl exerts on the $\delta^{13}\text{C}$ distribution.

Our standard and sensitivity simulations all reproduce well the geographic distribution of and temporal evolution of CH₄ observed at the GMD surface sites. However, imposing Cl distributions from a range of chemical transport models used in the scientific community leads to large differences in the simulated distribution of the $\delta^{13}\text{C}$ of CH₄. The CH₄ sinks from Cl in our SimStd and SimGC simulations are both below 1% of the total CH₄ sink, as suggested by Gromov et al. (2018). Yet the SimStd and SimGC simulations underestimate and overestimate, respectively, the observed $\delta^{13}\text{C}$ in 2004, despite the fact that both include only a relatively small CH₄ sink from Cl.

Our ability to reproduce the observed latitudinal distribution of $\delta^{13}\text{C}$ depends not only on the assumed value of global mean Cl, but also its geographic distribution. The detailed halogen chemistry model (TOMCAT) of Hossaini et al. (2016) places the maximum Cl values in the continental NH, in contrast to the large MBL Cl sink used in Allan et al. (2007) to explain SH observations. We find that the strong NH Cl maximum, along with the resulting reduction in OH fractionation required to maintain consistency with observations, acts to flatten the interhemispheric gradient of $\delta^{13}\text{C}$, while the MBL Cl sink increases the hemispheric differences in NH winter and also strengthens the seasonal cycle. However, the interhemispheric gradient is also influenced by spatial variation in the isotopic signatures of the sources and uncertainties in the soil sink, complicating this issue.

Two values for the fractionating effect of OH (α_{OH}) on $\delta^{13}C$ (Cantrell et al., 1990; Saueressig et al., 2001) are widely cited in the literature. Combining the TOMCAT Cl fields with the α_{OH} of Saueressig et al. (2001) leads to an underestimate of observed $\delta^{13}C$, but combining it with the Cantrell et al. (1990) α_{OH} would lead to an overestimate. Reducing uncertainty in the fractionating effect of OH would thus improve our ability to constrain the role of Cl.

Observations of the $\delta^{13}C$ of CH_4 provide an important tool for constraining the CH_4 budget. We find that the range of Cl fields available from current global models leads to a wide range of simulated $\delta^{13}C$ values. Each percent increase in the amount of CH_4 loss occurring by reaction with Cl increases global mean surface $\delta^{13}C$ of CH_4 by approximately 0.5‰. This relationship can be used to estimate the impact on methane's isotopic values from future model simulations of Cl. The choice of Cl field thus strongly impacts what CH_4 source mixture best fits $\delta^{13}C$ observations. Better quantification of the role of Cl in the methane budget and further developing models of tropospheric halogens is therefore critical for interpreting the $\delta^{13}C$ observations to their fullest potential.

Data Availability

The methane and $\delta^{13}CH_4$ observations are available from the NOAA GMD website: <https://www.esrl.noaa.gov/gmd/dv/data/>. Output from the GEOS model is on the NASA Center for Climate Simulation (NCCS) system.

Author Contributions

SS designed and conducted simulation, performed analysis, and prepared the manuscript. JSW contributed to model development and experiment design. MM contributed to model development. BD contributed to model development and conceptualization. RH and CK contributed inputs to the simulations. SM and JWCW contributed data and aided in its interpretation. All authors contributed to the editing and revising of the manuscript.

The authors declare no competing interests.

Acknowledgements

Computational resources were provided by the NASA Center for Climate Simulation (NCCS). The authors thank Prabir Patra for useful discussions. RH is supported by a NERC Independent Research Fellowship (NE/N014375/1).

References

- Allan, W., Manning, M. R., Lassey, K. R., Lowe, D. C., and Gomez, A. J.: Modeling the variation of $\delta^{13}C$ in atmospheric methane: Phase ellipses and the kinetic isotope effect, *Global Biogeochemical Cycles*, 15, 467-481, doi:10.1029/2000GB001282, 2001.
- Allan, W., Struthers, H., and Lowe, D.: Methane carbon isotope effects caused by atomic chlorine in the marine boundary layer: Global model results compared with Southern Hemisphere measurements, *Journal of Geophysical Research: Atmospheres*, 112, 2007.

369 Bock, M., Schmitt, J., Beck, J., Seth, B., Chappellaz, J., and Fischer, H.: Glacial/interglacial wetland, biomass
370 burning, and geologic methane emissions constrained by dual stable isotopic CH₄ ice core records, *Proceedings of*
371 *the National Academy of Sciences*, 114, E5778-E5786, 10.1073/pnas.1613883114, 2017.

372 Brownlow, R., Lowry, D., Fisher, R., France, J., Lanoisellé, M., White, B., Wooster, M., Zhang, T., and Nisbet, E.:
373 Isotopic ratios of tropical methane emissions by atmospheric measurement, *Global Biogeochemical Cycles*, 31,
374 1408-1419, 2017.

375 Cantrell, C. A., Shetter, R. E., McDaniel, A. H., Calvert, J. G., Davidson, J. A., Lowe, D. C., Tyler, S. C., Cicerone,
376 R. J., and Greenberg, J. P.: Carbon kinetic isotope effect in the oxidation of methane by the hydroxyl radical, *Journal*
377 *of Geophysical Research: Atmospheres*, 95, 22455-22462, 1990.

378 Craig, H.: Isotopic Standards for Carbon and Oxygen and Correction Factors for Mass-Spectrometric Analysis OF
379 Carbon Dioxide, *Geochimica Et Cosmochimica Acta*, 12, 133-149, 10.1016/0016-7037(57)90024-8, 1957.

380 Dlugokencky, E., Bruhwiler, L., White, J., Emmons, L., Novelli, P., Montzka, S., Masarie, K., Lang, P., Crotwell,
381 A., Miller, J., and Gatti, L.: Observational constraints on recent increases in the atmospheric CH₄ burden,
382 *Geophysical Research Letters*, 36, 10.1029/2009GL039780, 2009.

383 Dlugokencky, E., Nisbet, E., Fisher, R., and Lowry, D.: Global atmospheric methane: budget, changes and dangers,
384 *Philosophical Transactions of the Royal Society a-Mathematical Physical and Engineering Sciences*, 369, 2058-
385 2072, 10.1098/rsta.2010.0341, 2011.

386 Dlugokencky, E.J., P.M. Lang, A.M. Crotwell, J.W. Mund, M.J. Crotwell, and K.W. Thoning, *Atmospheric*
387 *Methane Dry Air Mole Fractions from the NOAA ESRL Carbon Cycle Cooperative Global Air Sampling Network,*
388 1983-2017, Version: 2018-08-01, Path: ftp://aftp.cmdl.noaa.gov/data/trace_gases/ch4/flask/surface/, 2018.

389 Duncan, B. N., Strahan, S. E., Yoshida, Y., Steenrod, S. D., and Livesey, N.: Model study of the cross-tropopause
390 transport of biomass burning pollution, *Atmospheric Chemistry and Physics*, 7, 3713-3736, 2007.

391 Elshorbany, Y. F., Duncan, B. N., Strode, S. A., Wang, J. S., and Kouatchou, J.: The description and validation of
392 the computationally Efficient CH₄-CO-OH (ECCOHv1.01) chemistry module for 3-D model applications,
393 *Geoscientific Model Development*, 9, 799-822, 10.5194/gmd-9-799-2016, 2016.

394 Etiope, G., and Milkov, A.: A new estimate of global methane flux from onshore and shallow submarine mud
395 volcanoes to the atmosphere, *Environmental Geology*, 46, 997-1002, 10.1007/s00254-004-1085-1, 2004.

396 European Commission, Joint Research Center (JRC)/Netherlands Environmental Assessment Agency (PBL).
397 Emission Database for Global Atmospheric Research (EDGAR), <http://edgar.jrc.ec.europa.eu>.

398 Ferretti, D. F., Miller, J. B., White, J. W. C., Etheridge, D. M., Lassey, K. R., Lowe, D. C., Meure, C. M. M., Dreier,
399 M. F., Trudinger, C. M., van Ommen, T. D., and Langenfelds, R. L.: Unexpected Changes to the Global Methane
400 Budget over the Past 2000 Years, *Science*, 309, 1714-1717, 10.1126/science.1115193, 2005.

401 Fischer, H., Behrens, M., Bock, M., Richter, U., Schmitt, J., Loulergue, L., Chappellaz, J., Spahni, R., Blunier, T.,
402 Leuenberger, M., and Stocker, T. F.: Changing boreal methane sources and constant biomass burning during the last
403 termination, *Nature*, 452, 864, 10.1038/nature06825
404 <https://www.nature.com/articles/nature06825#supplementary-information>, 2008.

405 Fung, I., John, J., Lerner, J., Matthews, E., Prather, M., Steele, L., and Fraser, P.: 3-Dimensional Model Synthesis of
 406 the Global Methane Cycle, *Journal of Geophysical Research-Atmospheres*, 96, 13033-13065, 10.1029/91JD01247,
 407 1991.
 408 Ganesan, A., Stell, A., Gedney, N., Comyn-Platt, E., Hayman, G., Rigby, M., Poulter, B., and Hornibrook, E.:
 409 Spatially Resolved Isotopic Source Signatures of Wetland Methane Emissions, *Geophysical Research Letters*, 45,
 410 3737-3745, 2018.
 411 Gelaro, R., McCarty, W., Suarez, M., Todling, R., Molod, A., Takacs, L., Randles, C., Darmenov, A., Bosilovich,
 412 M., Reichle, R., Wargan, K., Coy, L., Cullather, R., Draper, C., Akella, S., Buchard, V., Conaty, A., da Silva, A.,
 413 Gu, W., Kim, G., Koster, R., Lucchesi, R., Merkova, D., Nielsen, J., Partyka, G., Pawson, S., Putman, W.,
 414 Rienecker, M., Schubert, S., Sienkiewicz, M., and Zhao, B.: The Modern-Era Retrospective Analysis for Research
 415 and Applications, Version 2 (MERRA-2), *Journal of Climate*, 30, 5419-5454, 10.1175/JCLI-D-16-0758.1, 2017.
 416 Ghosh, A., Patra, P., Ishijima, K., Umezawa, T., Ito, A., Etheridge, D., Sugawara, S., Kawamura, K., Miller, J., and
 417 Dlugokencky, E.: Variations in global methane sources and sinks during 1910–2010, *Atmospheric Chemistry and*
 418 *Physics*, 15, 2595-2612, 2015.
 419 Granier, C., Bessagnet, B., Bond, T., D'Angiola, A., van der Gon, H. D., Frost, G. J., Heil, A., Kaiser, J. W., Kinne,
 420 S., Klimont, Z., Kloster, S., Lamarque, J. F., Lioussé, C., Masui, T., Meleux, F., Mieville, A., Ohara, T., Raut, J. C.,
 421 Riahi, K., Schultz, M. G., Smith, S. J., Thompson, A., van Aardenne, J., van der Werf, G. R., and van Vuuren, D. P.:
 422 Evolution of anthropogenic and biomass burning emissions of air pollutants at global and regional scales during the
 423 1980-2010 period, *Climatic Change*, 109, 163-190, 10.1007/s10584-011-0154-1, 2011.
 424 Gromov, S., Brenninkmeijer, C. A., and Jöckel, P.: A very limited role of tropospheric chlorine as a sink of the
 425 greenhouse gas methane, *Atmospheric Chemistry and Physics*, 18, 9831-9843, 2018.
 426 Hausmann, P., Sussmann, R., and Smale, D.: Contribution of oil and natural gas production to renewed increase in
 427 atmospheric methane (2007–2014): top–down estimate from ethane and methane column observations, *Atmospheric*
 428 *Chemistry and Physics*, 16, 3227-3244, 2016.
 429 Hopcroft, P. O., Valdes, P. J., and Kaplan, J. O.: Bayesian Analysis of the Glacial-Interglacial Methane Increase
 430 Constrained by Stable Isotopes and Earth System Modeling, *Geophysical Research Letters*, 45, 3653-3663,
 431 doi:10.1002/2018GL077382, 2018.
 432 Hossaini, R., Chipperfield, M. P., Saiz-Lopez, A., Fernandez, R., Monks, S., Feng, W., Brauer, P., and von Glasow,
 433 R.: A global model of tropospheric chlorine chemistry: Organic versus inorganic sources and impact on methane
 434 oxidation, *Journal of Geophysical Research: Atmospheres*, 121, 14,271-214,297, doi:10.1002/2016JD025756, 2016.
 435 Houweling, S., Kaminski, T., Dentener, F., Lelieveld, J., and Heimann, M.: Inverse modeling of methane sources
 436 and sinks using the adjoint of a global transport model, *Journal of Geophysical Research-Atmospheres*, 104, 26137-
 437 26160, 10.1029/1999JD900428, 1999.
 438 Houweling, S., Dentener, F., and Lelieveld, J.: Simulation of preindustrial atmospheric methane to constrain the
 439 global source strength of natural wetlands, *Journal of Geophysical Research-Atmospheres*, 105, 17243-17255,
 440 10.1029/2000JD900193, 2000.

441 Houweling, S., Van der Werf, G., Goldewijk, K. K., Röckmann, T., and Aben, I.: Early anthropogenic CH₄
 442 emissions and the variation of CH₄ and 13CH₄ over the last millennium, *Global Biogeochemical Cycles*, 22, 2008.
 443 Hu, L., Keller, C., Long, M., Sherwen, T., Auer, B., Da Silva, A., Nielsen, J., Pawson, S., Thompson, M., Trayanov,
 444 A., Travis, K., Grange, S., Evans, M., and Jacob, D.: Global simulation of tropospheric chemistry at 12.5 km
 445 resolution: performance and evaluation of the GEOS-Chem chemical module (v10-1) within the NASA GEOS Earth
 446 system model (GEOS-5 ESM), *Geoscientific Model Development*, 11, 4603–4620, 10.5194/gmd-11-4603-2018,
 447 2018.
 448 Ito, A., and Inatomi, M.: Use of a process-based model for assessing the methane budgets of global terrestrial
 449 ecosystems and evaluation of uncertainty, *Biogeosciences*, 9, 759–773, 10.5194/bg-9-759-2012, 2012.
 450 Kai, F., Tyler, S., Randerson, J., and Blake, D.: Reduced methane growth rate explained by decreased Northern
 451 Hemisphere microbial sources, *Nature*, 476, 194–197, 10.1038/nature10259, 2011.
 452 Kirschke, S., Bousquet, P., Ciais, P., Saunois, M., Canadell, J. G., Dlugokencky, E. J., Bergamaschi, P., Bergmann,
 453 D., Blake, D. R., Bruhwiler, L., Cameron-Smith, P., Castaldi, S., Chevallier, F., Feng, L., Fraser, A., Heimann, M.,
 454 Hodson, E. L., Houweling, S., Josse, B., Fraser, P. J., Krummel, P. B., Lamarque, J.-F., Langenfelds, R. L., Le
 455 Quere, C., Naik, V., O'Doherty, S., Palmer, P. I., Pison, I., Plummer, D., Poulter, B., Prinn, R. G., Rigby, M.,
 456 Ringeval, B., Santini, M., Schmidt, M., Shindell, D. T., Simpson, I. J., Spahni, R., Steele, L. P., Strode, S. A., Sudo,
 457 K., Szopa, S., van der Werf, G. R., Voulgarakis, A., van Weele, M., Weiss, R. F., Williams, J. E., and Zeng, G.:
 458 Three decades of global methane sources and sinks, *Nature Geoscience*, 6, 813–823, 10.1038/NGEO1955, 2013.
 459 Lassey, K. R., Etheridge, D. M., Lowe, D. C., Smith, A. M., and Ferretti, D. F.: Centennial evolution of the
 460 atmospheric methane budget: what do the carbon isotopes tell us?, *Atmos. Chem. Phys.*, 7, 2119–2139, 10.5194/acp-
 461 7-2119-2007, 2007.
 462 Long, M., Yantosca, R., Nielsen, J., Keller, C., da Silva, A., Sulprizio, M., Pawson, S., and Jacob, D.: Development
 463 of a grid-independent GEOS-Chem chemical transport model (v9-02) as an atmospheric chemistry module for Earth
 464 system models, *Geoscientific Model Development*, 8, 595–602, 10.5194/gmd-8-595-2015, 2015.
 465 McNorton, J., Chipperfield, M., Gloor, M., Wilson, C., Feng, W., Hayman, G., Rigby, M., Krummel, P., O'Doherty,
 466 S., Prinn, R., Weiss, R., Young, D., Dlugokencky, E., and Montzka, S.: Role of OH variability in the stalling of the
 467 global atmospheric CH₄ growth rate from 1999 to 2006, *Atmospheric Chemistry and Physics*, 16, 7943–7956,
 468 10.5194/acp-16-7943-2016, 2016.
 469 Mikaloff Fletcher, S. E., Tans, P. P., Bruhwiler, L. M., Miller, J. B., and Heimann, M.: CH₄ sources estimated from
 470 atmospheric observations of CH₄ and its 13C/12C isotopic ratios: 2. Inverse modeling of CH₄ fluxes from
 471 geographical regions, *Global Biogeochemical Cycles*, 18, doi:10.1029/2004GB002224, 2004a.
 472 Mikaloff Fletcher, S. E., Tans, P. P., Bruhwiler, L. M., Miller, J. B., and Heimann, M.: CH₄ sources estimated from
 473 atmospheric observations of CH₄ and its 13C/12C isotopic ratios: 1. Inverse modeling of source processes, *Global*
 474 *Biogeochemical Cycles*, 18, doi:10.1029/2004GB002223, 2004b.
 475 Molod, A., Takacs, L., Suarez, M., and Bacmeister, J.: Development of the GEOS-5 atmospheric general circulation
 476 model: evolution from MERRA to MERRA2, *Geoscientific Model Development*, 8, 1339–1356, 10.5194/gmd-8-
 477 1339-2015, 2015.

478 Monteil, G., Houweling, S., Dlugokenky, E., Maenhout, G., Vaughn, B., White, J., and Rockmann, T.: Interpreting
 479 methane variations in the past two decades using measurements of CH₄ mixing ratio and isotopic composition,
 480 *Atmospheric chemistry and physics*, 11, 9141-9153, 2011.
 481 Naik, V., Voulgarakis, A., Fiore, A. M., Horowitz, L. W., Lamarque, J. F., Lin, M., Prather, M. J., Young, P. J.,
 482 Bergmann, D., Cameron-Smith, P. J., Cionni, I., Collins, W. J., Dalsoren, S. B., Doherty, R., Eyring, V., Faluvegi,
 483 G., Folberth, G. A., Josse, B., Lee, Y. H., MacKenzie, I. A., Nagashima, T., van Noije, T. P. C., Plummer, D. A.,
 484 Righi, M., Rumbold, S. T., Skeie, R., Shindell, D. T., Stevenson, D. S., Strode, S., Sudo, K., Szopa, S., and Zeng,
 485 G.: Preindustrial to present-day changes in tropospheric hydroxyl radical and methane lifetime from the
 486 Atmospheric Chemistry and Climate Model Intercomparison Project (ACCMIP), *Atmospheric Chemistry and*
 487 *Physics*, 13, 5277-5298, 10.5194/acp-13-5277-2013, 2013.
 488 Nielsen, J., Pawson, S., Molod, A., Auer, B., da Silva, A., Douglass, A., Duncan, B., Liang, Q., Manyin, M., Oman,
 489 L., Putman, W., Strahan, S., and Wargan, K.: Chemical Mechanisms and Their Applications in the Goddard Earth
 490 Observing System (GEOS) Earth System Model, *Journal of Advances in Modeling Earth Systems*, 9, 3019-3044,
 491 10.1002/2017MS001011, 2017.
 492 Nisbet, E., Dlugokenky, E., Manning, M., Lowry, D., Fisher, R., France, J., Michel, S., Miller, J., White, J., and
 493 Vaughn, B.: Rising atmospheric methane: 2007–2014 growth and isotopic shift, *Global Biogeochemical Cycles*, 30,
 494 1356-1370, 2016.
 495 Nisbet, E., Manning, M., Dlugokenky, E., Fisher, R., Lowry, D., Michel, S., Myhre, C., Platt, M., Allen, G.,
 496 Bousquet, P., Brownlow, R., Cain, M., France, J., Hermansen, O., Hossaini, R., Jones, A., Levin, I., Manning, A.,
 497 Myhre, G., Pyle, J., Vaughn, B., Warwick, N., and White, J.: Very Strong. Atmospheric Methane Growth in the 4
 498 Years 2014-2017: Implications for the paris Agreement, *Global Biogeochemical Cycles*, 33, 318-342,
 499 10.1029/2018GB006009, 2019.
 500 Orbe, C., Oman, L., Strahan, S., Waugh, D., Pawson, S., Takacs, L., and Molod, A.: Large-Scale Atmospheric
 501 Transport in GEOS Replay Simulations, *Journal of Advances in Modeling Earth Systems*, 9, 2545-2560,
 502 10.1002/2017MS001053, 2017.
 503 Patra, P., Houweling, S., Krol, M., Bousquet, P., Belikov, D., Bergmann, D., Bian, H., Cameron-Smith, P.,
 504 Chipperfield, M., Corbin, K., Fortems-Cheiney, A., Fraser, A., Gloor, E., Hess, P., Ito, A., Kawa, S., Law, R., Loh,
 505 Z., Maksyutov, S., Meng, L., Palmer, P., Prinn, R., Rigby, M., Saito, R., and Wilson, C.: TransCom model
 506 simulations of CH₄ and related species: linking transport, surface flux and chemical loss with CH₄ variability in the
 507 troposphere and lower stratosphere, *Atmospheric Chemistry and Physics*, 11, 12813-12837, 10.5194/acp-11-12813-
 508 2011, 2011.
 509 Platt, U., Allan, W., and Lowe, D.: Hemispheric average Cl atom concentration from ¹³C/¹²C ratios in atmospheric
 510 methane, *Atmos. Chem. Phys.*, 4, 2393-2399, 10.5194/acp-4-2393-2004, 2004.
 511 Quay, P., King, S., Stutsman, J., Wilbur, D., Steele, L., Fung, I., Gammon, R., Brown, T., Farwell, G., Grootes, P.,
 512 and Schmidt, F.: Carbon Isotopic Composition of Atmospheric CH₄: Fossil and Biomass Burning Source Strenghts,
 513 *Global Biogeochemical Cycles*, 5, 25-47, 10.1029/91GB00003, 1991.

514 Rice, A. L., Butenhoff, C. L., Teama, D. G., Röger, F. H., Khalil, M. A. K., and Rasmussen, R. A.: Atmospheric
 515 methane isotopic record favors fossil sources flat in 1980s and 1990s with recent increase, *Proceedings of the*
 516 *National Academy of Sciences*, 113, 10791-10796, 2016.
 517 Rigby, M., Prinn, R. G., Fraser, P. J., Simmonds, P. G., Langenfelds, R. L., Huang, J., Cunnold, D. M., Steele, L. P.,
 518 Krummel, P. B., Weiss, R. F., O'Doherty, S., Salameh, P. K., Wang, H. J., Harth, C. M., Mühle, J., and Porter, L.
 519 W.: Renewed growth of atmospheric methane, *Geophysical Research Letters*, 35, doi:10.1029/2008GL036037,
 520 2008.
 521 Rigby, M., Montzka, S. A., Prinn, R. G., White, J. W., Young, D., O'Doherty, S., Lunt, M. F., Ganesan, A. L.,
 522 Manning, A. J., and Simmonds, P. G.: Role of atmospheric oxidation in recent methane growth, *Proceedings of the*
 523 *National Academy of Sciences*, 114, 5373-5377, 2017.
 524 Rotman, D., Tannahill, J., Kinnison, D., Connell, P., Bergmann, D., Proctor, D., Rodriguez, J., Lin, S., Rood, R.,
 525 Prather, M., Rasch, P., Considine, D., Ramarosan, R., and Kawa, S.: Global Modeling Initiative assessment model:
 526 Model description, integration, and testing of the transport shell, *Journal of Geophysical Research-Atmospheres*,
 527 106, 1669-1691, 10.1029/2000JD900463, 2001.
 528 Saueressig, G., Bergamaschi, P., Crowley, J., Fischer, H., and Harris, G.: Carbon Kinetic Isotope Effect in the
 529 Reaction of CH₄ with Cl Atoms, *Geophysical Research Letters*, 22, 1225-1228, 10.1029/95GL00881, 1995.
 530 Saueressig, G., Crowley, J. N., Bergamaschi, P., Brühl, C., Brenninkmeijer, C. A. M., and Fischer, H.: Carbon 13
 531 and D kinetic isotope effects in the reactions of CH₄ with O(1 D) and OH: New laboratory measurements and their
 532 implications for the isotopic composition of stratospheric methane, *Journal of Geophysical Research: Atmospheres*,
 533 106, 23127-23138, doi:10.1029/2000JD000120, 2001.
 534 Saunio, M., Bousquet, P., Poulter, B., Peregon, A., Ciais, P., Canadell, J. G., Dlugokencky, E. J., Etiope, G.,
 535 Bastviken, D., and Houweling, S.: The global methane budget 2000–2012, *Earth System Science Data (Online)*, 8,
 536 2016.
 537 Saunio, M., Bousquet, P., Poulter, B., Peregon, A., Ciais, P., Canadell, J., Dlugokencky, E., Etiope, G., Bastviken,
 538 D., Houweling, S., Janssens-Maenhout, G., Tubiello, F., Castaldi, S., Jackson, R., Alexe, M., Arora, V., Beerling,
 539 D., Bergamaschi, P., Blake, D., Brailsford, G., Bruhwiler, L., Crevoisier, C., Crill, P., Covey, K., Frankenberg, C.,
 540 Gedney, N., Hoglund-Isaksson, L., Ishizawa, M., Ito, A., Joos, F., Kim, H., Kleinen, T., Krummel, P., Lamarque, J.,
 541 Langenfelds, R., Locatelli, R., Machida, T., Maksyutov, S., Melton, J., Morino, I., Naik, V., O'Doherty, S.,
 542 Parmentier, F., Patra, P., Peng, C., Peng, S., Peters, G., Pison, I., Prinn, R., Ramonet, M., Riley, W., Saito, M.,
 543 Santini, M., Schroeder, R., Simpson, I., Spahni, R., Takizawa, A., Thornton, B., Tian, H., Tohjima, Y., Viovy, N.,
 544 Voulgarakis, A., Weiss, R., Wilton, D., Wiltshire, A., Worthy, D., Wunch, D., Xu, X., Yoshida, Y., Zhang, B.,
 545 Zhang, Z., and Zhu, Q.: Variability and quasi-decadal changes in the methane budget over the period 2000-2012,
 546 *Atmospheric Chemistry and Physics*, 17, 11135-11161, 10.5194/acp-17-11135-2017, 2017.
 547 Schaefer, H., Fletcher, S. E. M., Veidt, C., Lassey, K. R., Brailsford, G. W., Bromley, T. M., Dlugokencky, E. J.,
 548 Michel, S. E., Miller, J. B., Levin, I., Lowe, D. C., Martin, R. J., Vaughn, B. H., and White, J. W. C.: A 21st-century
 549 shift from fossil-fuel to biogenic methane emissions indicated by 13CH₄, *Science*, 352, 80-84,
 550 10.1126/science.aad2705, 2016.

551 Schwietzke, S., Sherwood, O., Ruhwiler, L., Miller, J., Etiopie, G., Dlugokencky, E., Michel, S., Arling, V., Vaughn,
 552 B., White, J., and Tans, P.: Upward revision of global fossil fuel methane emissions based on isotope database,
 553 *Nature*, 538, 88-91, 10.1038/nature19797, 2016.
 554 Sherwen, T., Schmidt, J. A., Evans, M. J., Carpenter, L. J., Großmann, K., Eastham, S. D., Jacob, D. J., Dix, B.,
 555 Koenig, T. K., Sinreich, R., Ortega, I., Volkamer, R., Saiz-Lopez, A., Prados-Roman, C., Mahajan, A. S., and
 556 Ordóñez, C.: Global impacts of tropospheric halogens (Cl, Br, I) on oxidants and composition in GEOS-Chem,
 557 *Atmos. Chem. Phys.*, 16, 12239-12271, 10.5194/acp-16-12239-2016, 2016.
 558 Sherwood, O., Schwietzke, S., Arling, V., and Etiopie, G.: Global Inventory of Gas Geochemistry Data from Fossil
 559 Fuel, Microbial and Burning Sources, version 2017, *Earth System Science Data*, 9, 639-656, 10.5194/essd-9-639-
 560 2017, 2017.
 561 Spivakovsky, C. M., Logan, J. A., Montzka, S. A., Balkanski, Y. J., Foreman-Fowler, M., Jones, D. B. A.,
 562 Horowitz, L. W., Fusco, A. C., Brenninkmeijer, C. A. M., Prather, M. J., Wofsy, S. C., and McElroy, M. B.: Three-
 563 dimensional climatological distribution of tropospheric OH: Update and evaluation, *Journal of Geophysical*
 564 *Research-Atmospheres*, 105, 8931-8980, 10.1029/1999jd901006, 2000.
 565 Strahan, S. E., Duncan, B. N., and Hoor, P.: Observationally derived transport diagnostics for the lowermost
 566 stratosphere and their application to the GMI chemistry and transport model, *Atmospheric Chemistry and Physics*, 7,
 567 2435-2445, 2007.
 568 Strahan, S. E., Douglass, A. R., and Newman, P. A.: The contributions of chemistry and transport to low arctic
 569 ozone in March 2011 derived from Aura MLS observations, *Journal of Geophysical Research: Atmospheres*, 118,
 570 1563-1576, 2013.
 571 Strobe, S., Duncan, B., Yegorova, E., Kouatchou, J., Ziemke, J., and Douglass, A.: Implications of carbon monoxide
 572 bias for methane lifetime and atmospheric composition in chemistry climate models, *Atmospheric Chemistry and*
 573 *Physics*, 15, 11789-11805, 2015.
 574 Tans, P.: A note on isotopic ratios and the global atmospheric methane budget, *Global Biogeochemical Cycles*, 11,
 575 77-81, 10.1029/96GB03940, 1997.
 576 Thompson, R., Nisbet, E., Pissot, I., Stohl, A., Blake, D., Dlugokencky, E., Helmig, D., and White, J.: Variability in
 577 Atmospheric Methane From Fossil Fuel and Microbial Sources Over the Last Three Decades, *Geophysical Research*
 578 *Letters*, 45, 11499-11508, 10.1029/2018GL078127, 2018.
 579 Thompson, R. L., Stohl, A., Zhou, L. X., Dlugokencky, E., Fukuyama, Y., Tohjima, Y., Kim, S. Y., Lee, H., Nisbet,
 580 E. G., and Fisher, R. E.: Methane emissions in East Asia for 2000–2011 estimated using an atmospheric Bayesian
 581 inversion, *Journal of Geophysical Research: Atmospheres*, 120, 4352-4369, 2015.
 582 Turner, A., Jacob, D., Benmergui, J., Wofsy, S., Maasackers, J., Butz, A., Hasekamp, O., and Biraud, S.: A large
 583 increase in US methane emissions over the past decade inferred from satellite data and surface observations,
 584 *Geophysical Research Letters*, 43, 2218-2224, 10.1002/2016GL067987, 2016.
 585 Turner, A. J., Frankenberg, C., Wennberg, P. O., and Jacob, D. J.: Ambiguity in the causes for decadal trends in
 586 atmospheric methane and hydroxyl, *Proceedings of the National Academy of Sciences*, 114, 5367-5372, 2017.

587 Tyler, S. C., Crill, P. M., and Brailsford, G. W.: $^{13}\text{C}^{12}\text{C}$ Fractionation of methane during oxidation in a temperate
 588 forested soil, *Geoschem. Cosmochem. Acta*, 58, 1625-1633, 10.1016/0016-7037(94)90564-9, 1994.
 589 Wang, J. S., McElroy, M. B., Spivakovsky, C. M., and Jones, D. B. A.: On the contribution of anthropogenic Cl to
 590 the increase in $\delta^{13}\text{C}$ of atmospheric methane, *Global Biogeochemical Cycles*, 16, 20-21-20-11, 2002.
 591 Wang, X., Jacob, D., Eastham, S., Sulprizio, M., Zhu, L., Chen, Q., Alexander, B., Sherwen, T., Evans, M., Lee, B.,
 592 Haskins, J., Lopez-Hilfiker, F., Thornton, J., Huey, G., and Liao, H.: The role of chlorine in global tropospheric
 593 chemistry, *Atmospheric Chemistry and Physics*, 19, 3981-4003, 10.5194/acp-19-3981-2019, 2019.
 594 Waugh, D., Crotwell, A., Dlugokencky, E., Dutton, G., Elkins, J., Hall, B., Hints, E., Hurst, D., Montzka, S.,
 595 Mondeel, D., Moore, F., Nance, J., Ray, E., Steenrod, S., Strahan, S., and Sweeney, C.: Tropospheric SF_6 : Age of
 596 air from the Northern Hemisphere midlatitude surface, *Journal of Geophysical Research-Atmospheres*, 118, 11429-
 597 11441, 10.1002/jgrd.50848, 2013.
 598 White, J.W.C., B.H. Vaughn, and S.E. Michel, University of Colorado, Institute of Arctic and Alpine Research
 599 (INSTAAR), Stable Isotopic Composition of Atmospheric Methane (^{13}C) from the NOAA ESRL Carbon Cycle
 600 Cooperative Global Air Sampling Network, 1998-2017, Version: 2018-09-24, Path:
 601 ftp://aftp.cmdl.noaa.gov/data/trace_gases/ch4c13/flask/, 2018.
 602 Worden, J. R., Bloom, A. A., Pandey, S., Jiang, Z., Worden, H. M., Walker, T. W., Houweling, S., and Röckmann,
 603 T.: Reduced biomass burning emissions reconcile conflicting estimates of the post-2006 atmospheric methane
 604 budget, *Nature communications*, 8, 2227, 2017.
 605 Zhang, Q.-L. and Li, W.-J.: A Calibrated Measurement of the Atomic Weight of Carbon, *Chinese Science Bulletin*
 606 35, 290, doi: 10.1360/sb1990-35-4-290, 1990.
 607
 608

609 **Table 1:** Emission source references and $\delta^{13}\text{C}$ values

Source	Reference	IAV	$\delta^{13}\text{C}$ (‰) ^a	CH ₄ Source (Tg yr ⁻¹) ^b
Animals (enteric fermentation)	EDGAR	Y	-62	102
C3 Biomass Burning (Forests)	MACCity	Y	-26	16
C4 Biomass Burning (Savannas)	MACCity	Y	-15	10
Coal, energy, and industry	EDGAR	Y	-35	6
Geologic (oil/gas/non-coal fuels, volcanos)	EDGAR, Transcom	Y, except volcanos	-40	124
Waste (solid and animal waste, wastewater)	EDGAR	Y	-55	74
Ocean	Transcom	N	-59	8
Rice	Visit model	Y	-63	44
Termites	Transcom	N	-57	22
Wetlands	Visit model	Y	-60	149

610 ^a $\delta^{13}\text{C}$ values from Dlugokencky et al., 2011; Lassey et al., 2007; Monteil et al., 2011; Houweling et al., 2000 and refs
611 therein

612 ^bValues for 2004

613 **Table 2:** Oxidants for the Standard and sensitivity simulations

Simulation	[CI] _{Trop} ^a (molec cm ⁻³)	CI Model ^b	CI Reference	OH modification ^c
SimStd	210	GMI	(Strahan et al., 2007; Rotman et al., 2001; Strahan et al., 2013; Duncan et al., 2007)	$\alpha = 0.9946$
SimGC	384	GEOSChem	(Sherwen et al., 2016)	$\alpha = 0.9946$
SimTom	1710	TOMCAT	(Hossaini et al., 2016)	-2% [OH] $\alpha = 0.9961$
SimTomB	1710	TOMCAT	(Hossaini et al., 2016)	$\alpha = 0.9946$
SimOHp	210	GMI	See SimStd	Not modified for 20% higher in NH
SimMBL	2810	Tanh function below 900hPa over ocean; GMI elsewhere	(Allan et al., 2007)	-4% [OH] $\alpha = 0.9961$

615 ^aConcentration of CI averaged over the troposphere

616 ^bName of the model that generated the offline CI field

617 ^cChanges to [OH] or α_{OH} compared to SimStd

618 **Table 3:** Observed and Simulated Interhemispheric Gradient in $\delta^{13}\text{C}$ -CH₄

	Jan. Gradient (‰) ^a	July Gradient (‰) ^a
GMD Obs	0.36	0.28
SimStd	0.17	0.11
SimGC	0.17	0.098
SimTom	0.051	0.010
SimMBL	0.30	0.13
SimOHp	0.22	0.15
SimWet	0.28	0.25

620 ^aAverage $\delta^{13}\text{C}$ -CH₄ at GMD site locations south of 30°S minus average $\delta^{13}\text{C}$ -CH₄ at locations north of 30°N

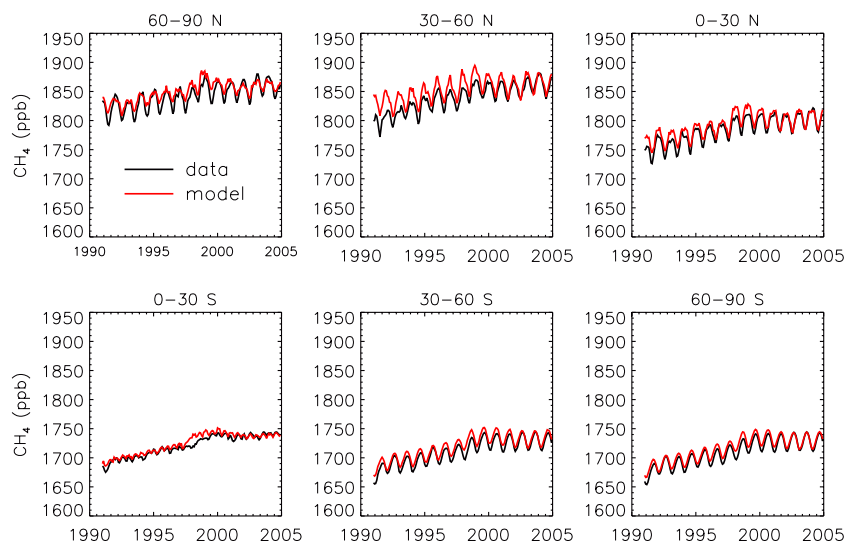


Fig 1: Monthly CH_4 observations from the GMD network (black) and simulated surface concentrations from SimStd (red) averaged over latitude bands

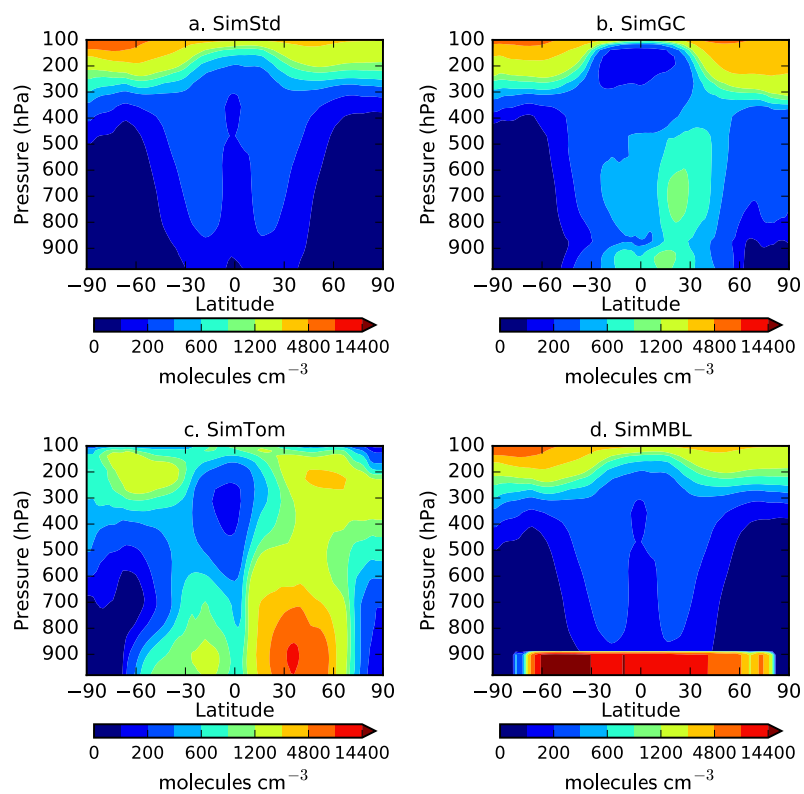


Fig. 2: Annual zonal mean CI field for a) SimStd, b) SimGC, c) SimTom, and d) SimMBL.

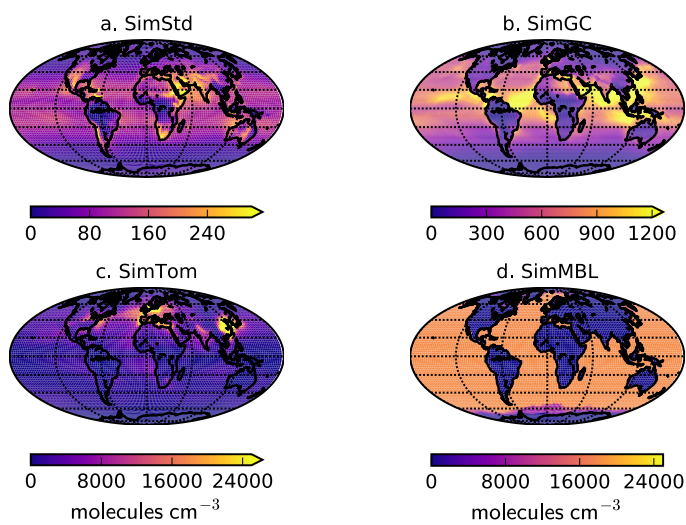


Fig. 3: Annual mean surface concentrations of Cl in a) SimStd, b) SimGC, c) SimTom, and d) SimMBL. Note the different color scales between panels.

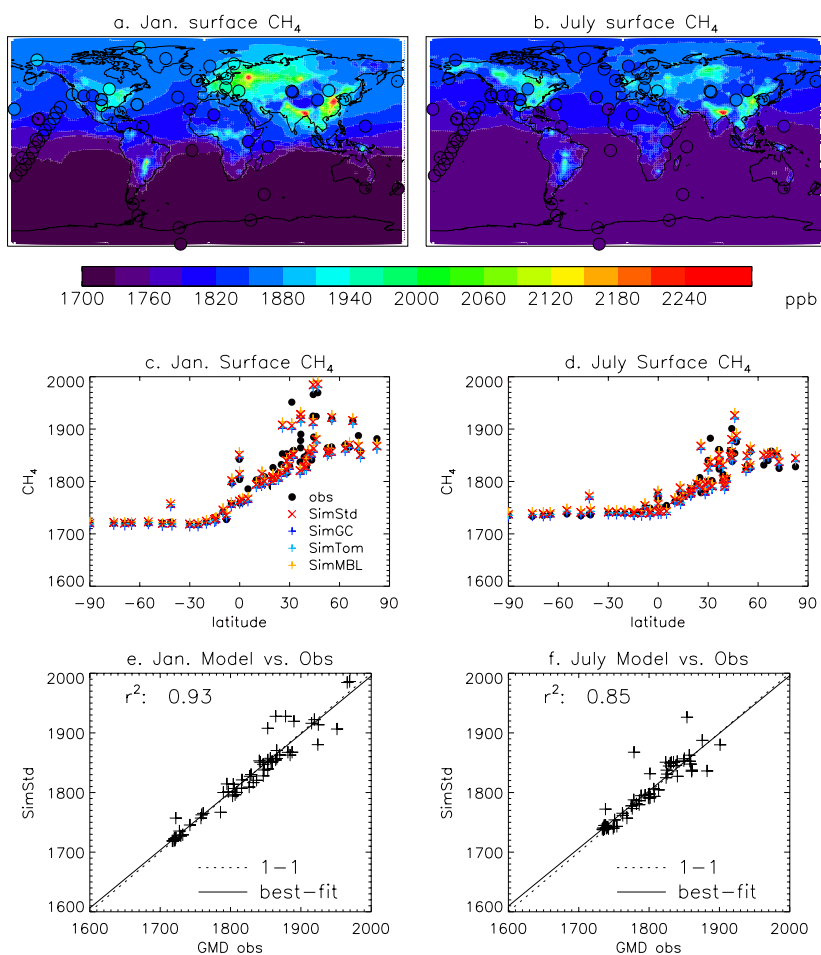


Fig. 4: Comparison of 2004 simulated and observed surface CH₄ concentrations for January (left) and July (right). a,b) Surface concentrations of CH₄ from SimStd are overplotted with the concentrations from the GMD observations in circles. c,d) GMD observations (black circles), SimStd (red x), SimGC (dark blue +), SimTom (light blue +), and SimMBL (orange +) CH₄ as a function of latitude. E,f) SimStd CH₄ (ppb) at the observation locations versus the GMD observations (+ signs) as well as the regression line (solid) and 1 to 1 line (dashed).

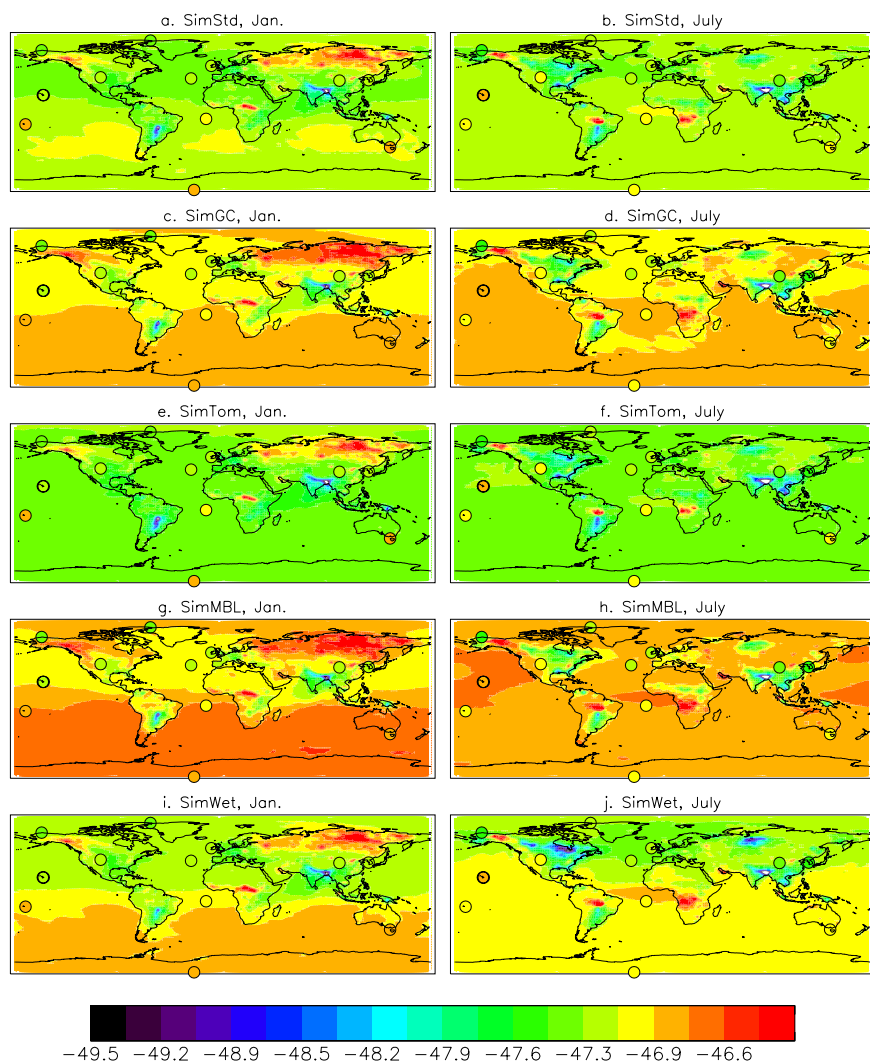


Fig. 5: Maps of the simulated surface $\delta^3\text{C}$ of CH_4 in per mil for Jan. (left) and July (right) overplotted with observations from the GMD sites (circles). The simulations are (a,b) SimStd, (c,d) SimGC, (e,f) SimTom, (g,h) SimMBL, and (i,j) SimWet.

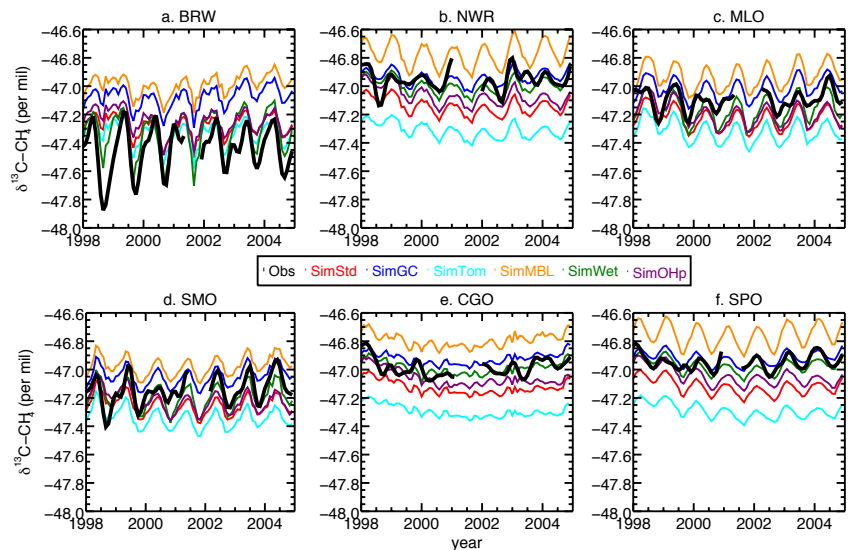


Fig. 6: The timeseries of observed (black) and simulated (colors) $\delta^{13}\text{CH}_4$ at the 6 GMD sites with records extending back to 1998. BRW: 71.3°N, 156.6°W; NWR: 40.0°N, 105.6°W; MLO: 19.5°N, 155.6°W; CGO: 40.7°S, 144.7°E and SPO: 90.0°S, 24.8°W.

Formatted: Font: 10 pt

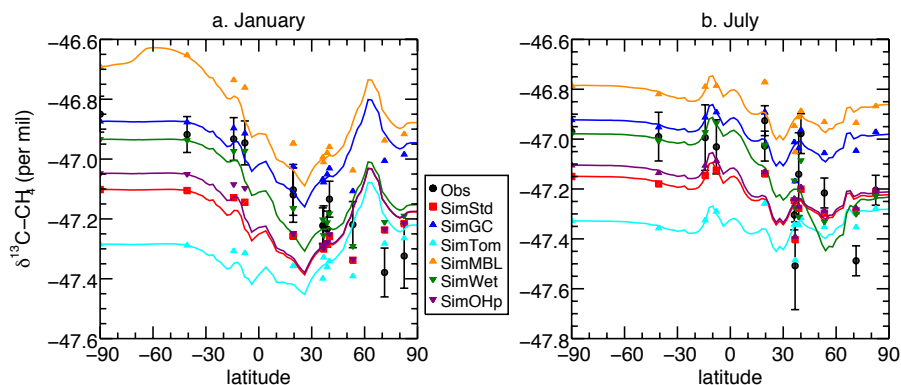


Fig. 7: $\delta^{13}\text{C}$ of CH_4 as a function of latitude in a) January and b) July 2004 for the GMD observations (Black circles), SimStd (red), SimGC (dark blue), SimTom (cyan), SimMBL (orange), SimWet (green), and SimOHp (purple). Errorbars represent the maximum of the analytical uncertainty (0.06‰) and the standard deviation of individual measurements in the month for each site. The colored lines represent the simulated zonal mean, while the colored symbols represent the simulation sampled at the location of the GMD observations.

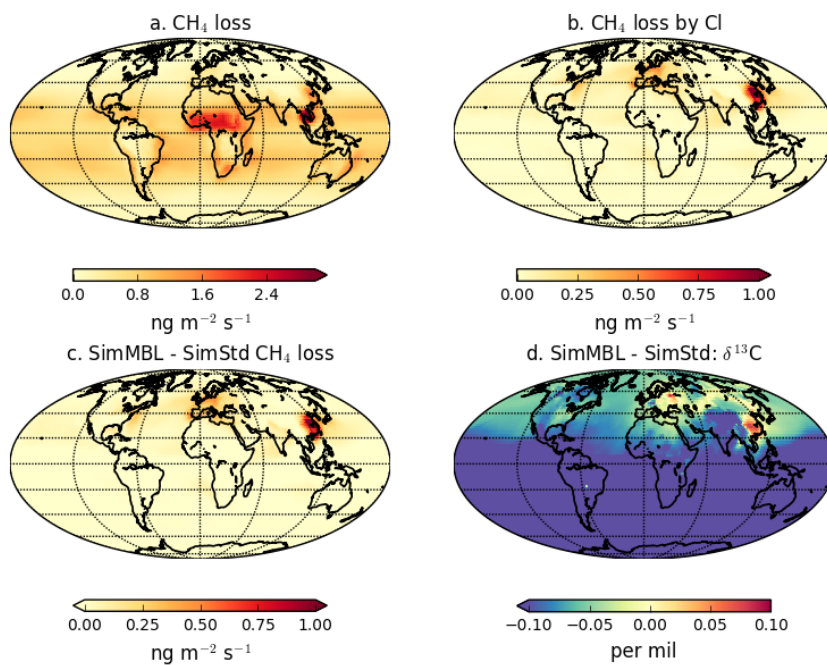


Fig 8: January a) CH_4 loss and b) CH_4 loss by Cl only in the SimTom simulation, as well as the difference in c) CH_4 loss and d) $\delta^{13}\text{C}\text{-CH}_4$ between the SimTom and SimStd simulations.

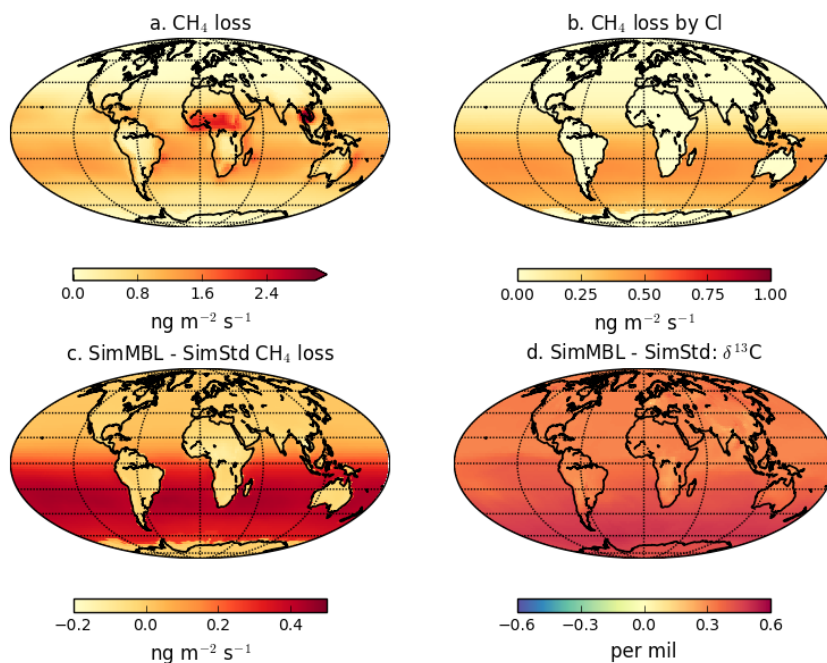


Fig 9: January a) CH_4 loss and b) CH_4 loss by Cl only in the SimMBL simulation, as well as the difference in c) CH_4 loss and d) $\delta^{13}\text{C}-\text{CH}_4$ between the SimMBL and SimStd simulations.

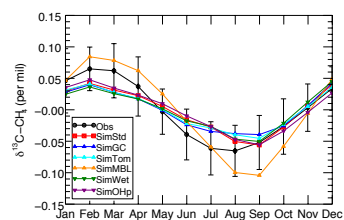


Fig. 10: The seasonal cycle of $\delta^{13}\text{C}$ of CH_4 at the SPO site with the annual mean removed averaged over 2002-2004 for the GMD observations (black), SimStd (red), SimGC (blue), SimTom (cyan), SimMBL (orange), SimWet (green), and SimOHp (purple). Errorbars represent the standard error, calculated as the maximum of the pooled standard deviation or the analytical uncertainty (0.06‰), divided by the square root of the number of years of observations.

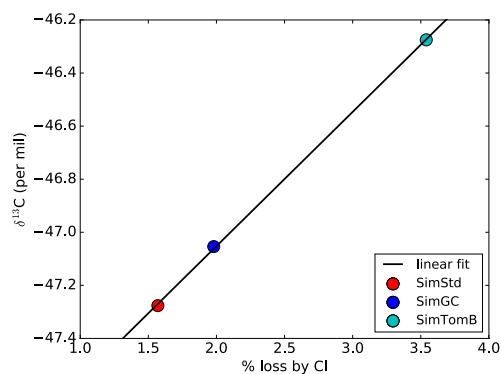


Fig. 11: Area-weighted global mean surface $\delta^{13}\text{C}$ for the SimStd (red), SimGC (blue) and SimTomB (cyan) simulations in 2004 as a function of the percent of CH_4 loss occurring by reaction with Cl. The linear best-fit line is shown in black.